INTERNATIONAL JOURNAL OF CLIMATOLOGY
Int. J. Climatol. (2009)
Published online in Wiley InterScience
(www.interscience.wiley.com) DOI: 10.1002/joc.1900

RMetS
Royal Meteorological Society

Variability and trends in the directional wave climate of the Southern Hemisphere

Mark A. Hemer,[a]* John A. Church[a,b] and John R. Hunter[b]
[a] *Centre for Australian Weather and Climate Research, CSIRO Marine and Atmospheric Research, Hobart TAS, Australia*
[b] *Antarctic Climate and Ecosystems Co-operative Research Centre, University of Tasmania, Hobart, TAS, Australia*

ABSTRACT: The effect of interannual climate variability and change on the historic, directional wave climate of the Southern Hemisphere is presented. Owing to a lack of *in situ* wave observations, wave climate in the Southern Hemisphere is determined from satellite altimetry and global ocean wave models. Altimeter data span the period 1985 to present, with the exception of a 2-year gap in 1989–1991. Interannual variability and trends in the significant wave height are determined from the satellite altimeter record (1991 to present), and the dominant modes of variability are identified using an empirical orthogonal function (EOF) analysis. Significant wave heights in the Southern Ocean are observed to show a strong positive correlation with the Southern Annular Mode (SAM), particularly during Austral autumn and winter months. Correlation between altimeter derived significant wave heights and the Southern Oscillation Index is observed in the Pacific basin, which is consistent with several previous studies.

Variability and trends of the directional wave climate are determined using the ERA-40 Waves Re-analysis for the period 1980–2001. Significant wave height, mean wave period and mean wave direction data are used to describe the climate of the wave energy flux vector. An EOF analysis of the wave energy flux vector is carried out to determine the dominant modes of variability of the directional seasonal wave energy flux climate. The dominant mode of variability during autumn and winter months is strongly correlated to the SAM. There is an anti-clockwise rotation of wave direction with the southward intensification of the Southern Ocean storm belt associated with the SAM. Clockwise rotation of flux vectors is observed in the Western Pacific Ocean during El-Nino events.

Directional variability of the wave energy flux in the Western Pacific Ocean has previously been shown to be of importance to sand transport along the south-eastern Australian margin, and the New Zealand region. The directional variability of the wave energy flux of the Southern Ocean associated with the SAM is expected to be of importance to the wave-driven currents responsible for the transport of sand along coastal margins in the Southern Hemisphere, in particular those on the Southern and Western coastal margins of the Australian continent.

KEY WORDS surface ocean waves; wave direction; Southern Ocean; Southern Annular Mode; climatology; coastal longshore transport

Received 10 June 2008; Revised 16 November 2008; Accepted 28 February 2009

1. Introduction

The surface ocean wave climate of the Southern Hemisphere (SH) has been largely understudied in ocean-scale regional wave climate studies. The predominant focus of such wave studies has focussed on high shipping regions of the North Atlantic (e.g. Bacon and Carter, 1991; Swail and Cox, 2000; Woolf *et al*., 2002; Wolf and Woolf, 2006), and the Northern Hemisphere as a whole (e.g. Graham, 2003; Wang and Swail, 2001; Sasaki *et al*., 2005). Description of the wave climate of the SH is limited to a few regional studies (e.g. Short and Trenaman, 1992; Laing, 2000; Scott *et al*., 2002; Gorman *et al*., 2003; Hemer *et al*., 2008), and global studies, where the attention paid to the SH is limited (e.g. Young, 1999; Cox and Swail, 2001; Sterl and Caires, 2005). It is widely understood however, after the early work by Snodgrass *et al*. (1966), that the swell generated in the Southern Ocean during intense Southern Ocean extra-tropical cyclones propagate throughout the World's oceans, impacting on almost all of the World's coasts.

Surface ocean waves play a significant role in the processes at the air–sea interface, and the adjacent boundary layers: the ocean surface mixed layer, and the atmosphere marine boundary layer. Consequently, waves impact upon surface winds, surface currents, turbulent mixing in the surface mixed layer and consequently the transport of heat, momentum and freshwater. Ocean waves also impact on the albedo of the ocean, thus impacting the radiative properties of the sea surface (Swail *et al*., 2001). Given the importance of the Southern Ocean to the global ocean, a more concerted effort is required to determine the variability and trends in the

* Correspondence to: Mark A. Hemer, Centre for Australian Weather and Climate Research, CSIRO Marine and Atmospheric Research, Hobart TAS, Australia. E-mail: mark.hemer@csiro.au

wave climate of the SH, and in particular the Southern Ocean.

The Southern Annular Mode (SAM) (also referred to as the high-latitude mode and the Antarctic Oscillation) is the principal mode of variability in the atmospheric circulation of the SH extratropics and high latitudes (Marshall, 2003). It is a zonally symmetric mode of variability with opposing geopotential height perturbations of opposite signs over the Antarctic and a zonal band centred near 45 °S (Gillett *et al*. 2006). Several papers have reported a trend in the SAM towards its positive phase, that is, when pressures over Antarctica are relatively low compared with those in the mid-latitudes (e.g. Kidson, 1999; Gong and Wang, 1999; Marshall, 2003). A number of regional studies have identified an influence of the SAM on winds (a poleward intensification of the Southern Ocean storm belt (Simmonds and Keay, 2000), and increased winds over the Southern Ocean by about 20% over the last 20 years (Hurrell and van Loon 1994; Thompson and Solomon 2002; Gillett *et al*., 2006); precipitation and temperature (Gillett *et al*., 2006).

A strong relationship between the Northern Annular Mode, or North Atlantic Oscillation, and the wave climate in the North Atlantic Ocean was described by Woolf *et al*. (2002), but little or no attention has been paid to effects of the SAM on the waves in the SH, and, in particular, the Southern Ocean. However, the variability of the SH wave climate has important implications for the global oceans. The global empirical orthogonal function (EOF) analysis of corrected ERA-40 re-analysed significant wave height data carried out by Sterl and Caires (2005) indicated that 15% of the global wave variability is due to the swell propagating from the SH storm track region, and it governs the variability of the global mean. Hence, it is important that the drivers of this Southern Ocean variability are understood. Data other than that derived from global wave models are sparse in the Southern Ocean, with very few waverider buoy records in the SH relative to the Northern Hemisphere. The most useful dataset for determining the variability in wave heights is derived from satellite altimeters, which is now of sufficient length to describe interannual variability of the wave climate. In this study, we use this data to describe the trends and variability of the Southern Ocean wave heights.

An aspect of the wave re-analysis dataset, which has been understudied, is the wave direction. Wave direction data are particularly sparse in the SH, with very few (less than 20% in the Australian region) of the waverider buoys in the region capable of measuring wave direction. Although station derived sea-level pressure based indices have been used as proxies for wave direction (e.g. Goodwin, 2005), global wave models provide the most useful dataset capable of providing some indication of the variability and trends of wave direction in the SH. The variability of wave direction is perhaps the most important of parameters to determine the influence of a changing wave climate on the coastal zone, altering longshore drifts and consequently coastal sand budgets. In this study, we use data from the global ERA-40 re-analysis (and corrected dataset) to describe the trends and variability of the directional Southern Ocean wave climate.

The aims of the paper are to describe the interannual variability and trends of the surface ocean waves in the SH, using available datasets, and determine the principle drivers of the variability. The paper is presented in five sections. This introduction is followed by a presentation of the datasets used (Section 2); a description of the variability and trends of SH surface ocean wave heights using the altimeter data (Section 3); a description of the variability and trends of the SH directional wave climate using the re-analysis data (Section 4) and Section 5 contains conclusions of the manuscript.

2. Datasets

2.1. Altimeter derived significant wave height (H_S)

Altimeter data have been obtained from the TUDelft RADS database (Naeije *et al*., 2000). Data from the Geosat, ERS-1, ERS-2, TOPEX/Poseidon, Jason, ENVISAT, and GFO missions are available. In this study, we only use data from the similar Ku-band altimeters of Geosat, ERS-1, ERS-2, TOPEX, Jason, ENVISAT and GFO. However, Geosat data available from RADS are unsuitable, as the available masking, and H_S standard deviation data is unavailable. Consequently Geosat data (i.e. altimeter data pre 1990) have been derived from elsewhere, as discussed below. The RADS database allows user-defined editing in order to select data according to a range of quality flags (as included in original Geophysical Data Records, GDR). In this study, all flagged data were rejected. Data were further rejected if the radar backscatter was less than 0 dB or greater than 20 dB (indicating non-ocean-like altimeter returns), or wave heights were greater than 25 m, or identically equal to 0, or whose standard deviation in wave heights was 0 or greater than 0.1 m (high values indicating returns may be contaminated by rain).

The most severe limitation of satellite altimetry is the sparseness of data as the satellite takes at least 10 days to return to the same point, and only the sea surface directly beneath the satellite is measured. Woolf *et al*. (2002) indicate that a reliable, satellite-derived wave climatology requires calibration of the altimeter significant wave heights using reliable *in situ* measurements, data screening to remove erroneous data, and attention to the sparse-sampling problem. In this study, we have used the same methods described by Woolf *et al*. (2002) to determine their satellite wave climatology, but the extra years and additional satellite missions extend this dataset. Owing to the problems previously mentioned with Geosat data, and their being no additional missions for this early period, the pre-1990 satellite wave climatology has been taken from the Woolf *et al*. study.

DOI: 10.1002/joc

The ocean was divided into a 2×2 grid (degrees longitude $\times$ degrees latitude), and wave data from each pass over through each grid cell were averaged to determine mean significant wave height, H_S, for every month of record for each grid cell. The seasonal climate is then described by averaging the results for each calendar month across all years (e.g. Young, 1999). Cotton and Carter (1994) established that only five valid calibrated satellite passes over a region of the ocean within a month were sufficient to obtain a reasonable accurate and unbiased estimate of the mean wave climatology in that month. Woolf *et al*. (2002) indicate that this condition was generally satisfied each month by each satellite for all 2×2 grid squares within its orbit.

As for Woolf *et al*., the calibration procedures used to correct the nominal altimeter derived wave heights to derive the climatology used in this study are described by Cotton (1998), Challenor and Cotton (2002) and Queffeulou (2004), and have been validated against the Australian waverider buoys by Hemer *et al*. (2007). Table I summarizes the calibration equations and the periods for which each satellite provides a validated climatology (Note that Woolf *et al*. (2002) present the TOPEX A-Side correction incorrectly. Their presentation is inconsistent with the referenced (Challenor and Cotton, 2002)) version presented here.). The resultant dataset used is a monthly $2^\circ \times 2^\circ$ gridded surface wave climatology of sufficient accuracy for describing the variability and trends of the SH wave climate. The Geosat data span the period December 1985–March 1989 (taken from the Woolf *et al*. study), and the remainder of the time-series span the period August 1991–December 2006.

Sporadic gaps in the climatology occur for a few grid squares in occasional months due to the sparse sampling by the altimeter. In this study, as for the Woolf *et al*. (2002) study, we are interested in the large-scale variability of the surface ocean wave climate, and the analysis requires data for every grid square for all months. Therefore, data were interpolated and smoothed using a 5 cell $\times$ 5 cell digital filter approximating Gaussian smoothing with a radius (standard deviation) of 2.8°.

2.2. ERA-40 Re-analysis global wave model data

The ERA-40 re-analysis wave model output is freely available on a 2.5° grid, providing significant wave height (H_S), mean wave period (T_M) and direction for the period 1958–2001. This dataset provides the ability to determine trends and variability in wave direction in the SH. However, Caires and Sterl (2005) found that the ERA-40 wave re-analysis tended to underestimate large wave heights, particularly in the Southern Ocean, and so they produced a statistically corrected dataset, which we call the corrected ERA-40 (C-ERA40) wave height data, at 1.5° resolution.

To describe directional wave data, we have converted the C-ERA-40 H_S data, and ERA T_M data (bi-linearly interpolated onto the 1.5° grid) into an energy flux, according to Holthuijsen (2007):

$$E_F = EC_G = \rho g \; {H_S}^2 \; C_G/16 \tag{1}$$

Where E is the wave energy density, C_G is the group wave speed (Holthuijsen, 2007), g is the gravitational acceleration and ρ is water density. Being a surface ocean wave energy flux, direction is given by the direction the waves are travelling. We define the wave energy flux to have direction equal to the ERA-40 mean wave direction. Eastward and Northward components of the energy flux (E_{fu} and E_{fv}, respectively) are then determined.

2.3. Waverider buoy data

Before detailing the variability and trends of the directional wave climate, confidence in the mean wave direction data available must be established. Very few directional waverider buoy data of sufficient length to describe trends and interannual variability are available in the SH. Directional data are available from six sites located on open coastline (i.e. not sited landward of the Great Barrier Reef, or landward of offshore islands) in Australia. Directional wave data were also obtained from the Banks Peninsula waverider buoy from the east coast of the south island of New Zealand. Only six of these seven buoys have data during the period of the ERA-40 re-analysis (The Western Australia Rottnest deployment commenced

Table I. Summary of Altimeter datasets and wave height calibrations.

Altimeter	Calibration	Dates	Reference
Geosat	Taken from Woolf *et al*. (2002)	12/1985–3/1989	Woolf *et al*. (2002)
ERS-1	$H_{real} = 1.109H_{ERS-1} + 0.334$	8/1991–6/1996	Challenor and Cotton (2002)
ERS-2	$H_{real} = 1.061H_{ERS-2} + 0.035$	4/1995–12/2006	Challenor and Cotton (2002)
TOPEX A	$H_{real} = 1.052H_{TOPEX} - 0.094 - 0.0004D$	9/1992–8/2002	Challenor and Cotton (2002)
TOPEX B	$H_{real} = 1.052H_{TOPEX} - 0.094$	9/2002–10/2005	Challenor and Cotton (2002)
JASON	$H_{real} = 1.059H_{JASON} - 0.057$	1/2002–12/2006	Queffeulou (2004)
GFO	$H_{real} = 1.0625H_{GFO} + 0.075$	1/2002–12/2006	Queffeulou (2004)
ENVISAT	$H_{real} = 1.0526H_{ENVISAT} - 0.199$	9/2002–12/2006	Queffeulou (2004)

H_{real} refers to a buoy-equivalent significant wave height, scaled from each altimeter dataset. Coefficients from referenced papers have been inverted where necessary.

D – the term in the calibration for TOPEX A is the number of days since 26/9/1996, and has the value of zero prior to 26/9/1996.

DOI: 10.1002/joc

Table II. Summary of directional waverider buoys used to validate ERA-40 wave direction in the Australian/New Zealand region.

Site name	Latitude (°S)	Longitude (°E)	Water Depth	Date direction commenced	Final date available
Brisbane	27.49	153.62	70	Jan-1997	Mar-2006
Tweed River	28.18	153.58	25	Jan-1997	Mar-2006
Byron Bay	28.82	153.73	71	Jan-2000	Dec-2004
Sydney	33.78	151.42	85	Jan-1993	Dec-2005
Batemans Bay	35.71	150.34	73	Jan-2001	Dec-2005
Banks Peninsula	43.75	173.33	76	Feb-1999	Dec-2006

in July 2005). The six buoy records used to validate ERA-40 mean wave direction data are summarized in Table II.

Monthly mean wave direction was determined by vector averaging unit vectors pointing in the wave direction. The long-term mean wave direction was similarly determined for each dataset (buoy and ERA-40). All of the directional waverider buoys are located in mid-water depths (~50–100 m) at which swell waves may interact with the seabed. Thus, before the waves have reached the buoy, they are likely to have undergone refraction and shoaling effects as they propagate from deep water onto the continental shelf. For validation of wave direction, refraction must be taken into account. Consequently, buoy wave directions have been inversely ray-traced into deep-water (utilizing Geoscience Australia's 0.01° bathymetry dataset; Petkovic and Buchanan, 2002). Data comparisons between ERA-40 wave direction and inverse ray-traced buoy measured wave direction were made (Table III), enabling a bias to be determined between datasets. The long-term mean was subtracted from the time series to compare the variability of wave direction (Figure 1). A bias exists between ERA-40 data and waverider buoy wave directions. For all stations except Brisbane the ERA-40 data display a greater southerly component (Table III). However, directional variability on seasonal and interannual time-scales shows good comparison. ERA-40 displays slightly greater variability in wave direction than the buoy data at most stations (Table III) but datasets are in phase with each other (Figure 1). At the buoys, which are available for directional comparisons, the wave signal is dominated by locally generated waves (deep-water waves). The ERA-40 dataset archives mean wave period, as opposed to peak wave period. Given the sea signal dominates the swell signal, the mean wave period is typically longer than the peak wave period, and the refraction estimates presented are likely an overestimate of the waves of peak energy. At the Sydney buoy, the overestimation of refraction is up to approximately 12° at times when there is a large discrepancy between mean and peak wave periods.

Table III. Comparison of ERA-40 wave direction and inverse ray-traced buoy wave directions.

Site	N	$\overline{\theta}_{\mathrm{ERA40}}$	$\overline{\theta}_{\mathrm{BUOY}}$	σ_{ERA40}	σ_{BUOY}
Banks Peninsula, NZ	26	134.7	124.3	0.43	0.46
Brisbane	61	94.5	110.1	0.21	0.27
Tweed	60	131.3	90.0	0.24	0.18
Byron Bay	24	140.5	133.1	0.26	0.21
Sydney	101	138.6	125.3	0.39	0.27
Batemans Bay	12	133.5	122.7	0.24	0.17

Means (indicated by the overbar) and standard deviations (indicated by σ). N is the number of months over which records were compared. Units of degrees from north.
σ is standard deviation of wave direction, determined from a unit vector of given direction. i.e. $\sigma = \sigma(\cos\theta) + \sigma(\sin\theta)$. This has a minimum value of 0 (indicating no variability), and a maximum value of 1 (indicating no directional coherence).

2.4. Climate indices

The relationships between wave climate and the Southern Oscillation Index (SOI, Figure 2), the Southern Annular Mode Index (SAMI, Figure 2; Marshall, 2003), the Indian Ocean Dipole (IOD; Saji *et al*., 1999) have been determined. No significant relationships were found to the IOD. The wave record used in this study is too short to establish significant correlation statistics to the Interdecadal Pacific Oscillation (IPO; Power *et al*., 1999); however, given the strong relationship between mean wave direction in the Tasman Sea and the IPO (Goodwin, 2005), it could be expected that this index is important for larger regions of the SH. This has not been investigated in this study.

3. Variability and trends of altimeter-measured significant wave heights

The annual cycle of altimeter derived H_S was determined from the mean for each month over all available years of data. There are 18 full years of data (1986–1988, 1992–2006), with an extra sample of each month for August–March, and a further one for December. However, to avoid any inconsistencies, which may exist between the Geosat climatology outlined by Woolf *et al*. and the climatology determined in this study, we concentrate on the data post-August 1991 for describing the mean annual cycle of significant wave height.

Seasonal mean significant wave heights were determined by combining the Dec-Jan-Feb (DJF) monthly means for summer, Mar-Apr-May (MAM) for Autumn, Jun-Jul-Aug (JJA) for Winter, and Sep-Oct-Nov (SON) for Spring. Finally, the mean significant wave height from

DOI: 10.1002/joc

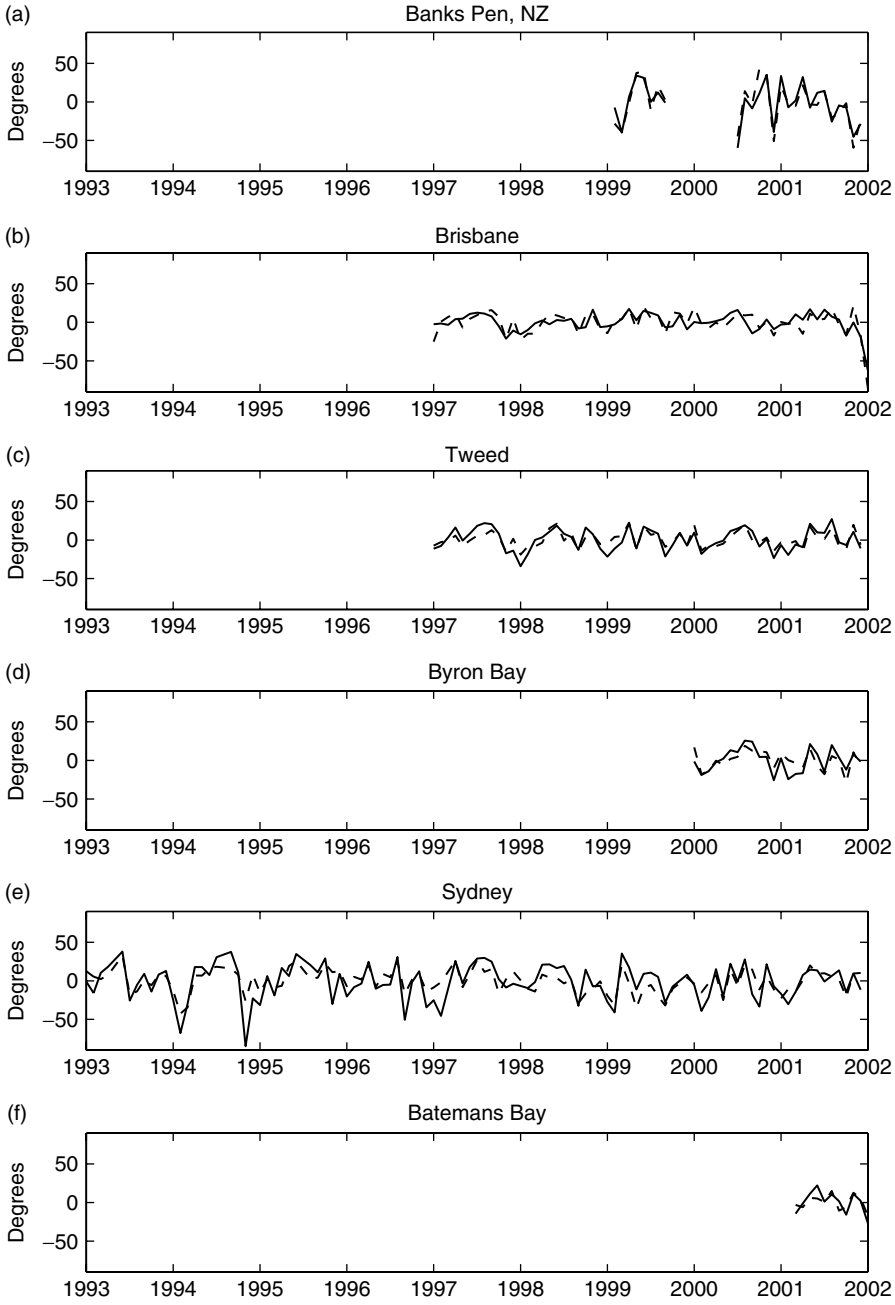

Figure 1. Comparison of wave directional anomalies between ERA-40 (dashed line) and inverse ray-traced buoy record (solid line) from (a) Banks Peninsula; (b) Brisbane; (c) Tweed; (d) Byron Bay; (e) Sydney; (f) Batemans Bay.

all satellites was then found by combining the individual monthly means into an all-seasons mean, with each month being equally weighted. The wave climatology described by the new dataset (not shown) is consistent with previous global wave climatologies (e.g. Young, 1999; Sterl and Caires, 2005). This climatology includes only the SH, and we see a strong latitudinal variation in H_S, with largest wave heights ($H_S \sim 5$ m) observed in the winter months JJA, in the Indian Ocean Sector of the Southern Ocean.

Interannual standard deviation of altimeter-measured H_S was determined by calculating the standard deviation of the monthly mean values. Interannual variability is greatest in the Indian Ocean Sector of the Southern Ocean, during the winter months. The high interannual variability observed in the monthly statistics suggests coherent processes may be acting to force this variability. We have investigated the relationship between the monthly mean altimeter-measured H_S anomalies with various climate indices.

Gridded values of mean altimeter measured H_S have been regressed against the Southern Oscillation (SO) and SAM climate indices, for each season (DJF, MAM, JJA, SON). A significant negative correlation is observed between the SOI and H_S in the western tropical Pacific for all seasons except DJF (when there is a negative correlation in the eastern Pacific), and on the Australian east coast during winter (JJA; Figure 3). Significant

DOI: 10.1002/joc

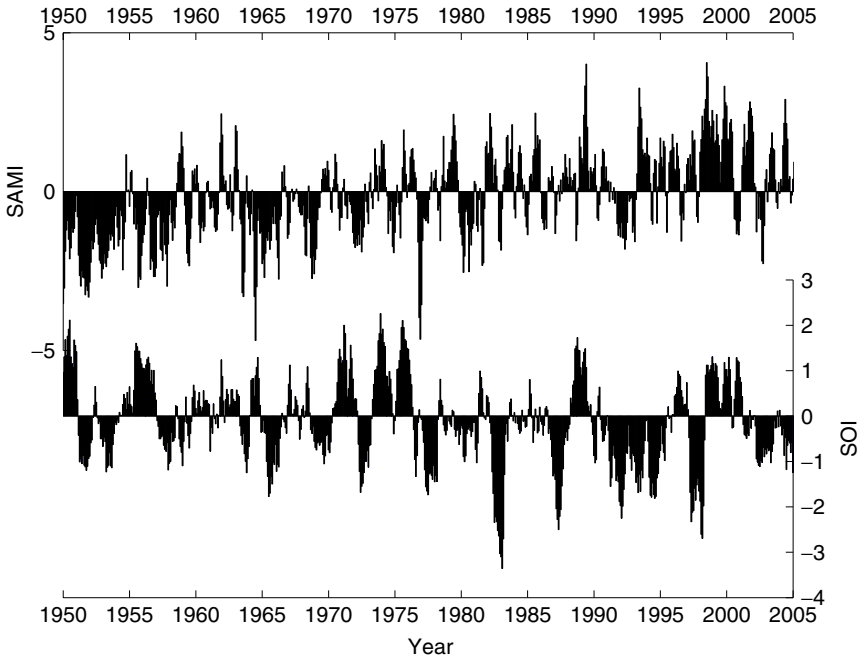

Figure 2. Three-month running mean Southern Annular Mode Index (upper, Marshall, 2003) and Southern Oscillation Index (lower). This figure is available in colour online at www.interscience.wiley.com/ijoc

positive correlation to the SO is observed off the western Australia coast during summer (DJF). This relationship between significant wave height and the SOI in the South Western Pacific Ocean (the Tasman and Coral Seas) has been previously described by Laing (2000).

Regression of seasonal mean H_S against seasonal means of the SAM shows a strong positive correlation between the SAM and autumn/winter H_S in the Indian and Pacific Ocean sectors of the Southern Ocean, and the Pacific Ocean tropical waters (Figure 4). During spring and summer, significant correlation to the SAM is observed only in the high latitudes. The SAM was detrended prior to determining regression statistics to ensure correlation between variability was being determined.

The time series of SH monthly mean significant wave height (Figure 5) illustrates the constant bias present between the early Geosat data, and the later data, which comes about as a result of differences in the processing procedure carried out in the two studies. Consequently, we concentrate on the post-1992 record for checking trends in wave heights. Monthly mean values of H_S have been regressed against time for each calendar month for two datasets: one spanning 1985–2006 (including the 1985–1989 Geosat data; Figure not shown), and the other spanning 1991–2006 (removing the Geosat data; Figure 6). This was done as inconsistencies (a constant offset) exist between the Woolf *et al*. climatology, and that determined in this study. We find significant positive trends in altimeter-measured H_S in the Southern Ocean during winter months (in particular July and September) between 1991 and 2006. These trends are observed over the whole Southern Ocean, and are typically greater (∼5 cm/yr) in the Indian and Pacific sectors. An exception occurs during July and August, when larger trends are observed in the South Atlantic (Figure 6). The trends analysis which includes the Geosat data displays spatial patterns analogous to the trends displayed in Figure 6; however, trends are not as great (∼1–2 cm/a) and not significant. Both datasets display a significant negative trend in the Indonesian Archipelago; however, care should be taken in interpreting these results where large errors may occur through land-affected data points.

The spatial pattern of the positive trend in altimeter-measured H_S in the Southern Ocean is consistent with the pattern of significant correlation between winter H_S and the SAMI (Figure 3) and the apparent trend in the SAM (Figure 2). The observed trend in the Southern Ocean altimeter-measured significant wave heights is consistent with a southward shift of the Southern Ocean storm belt, leading to stronger westerly winds, driving larger wave heights in the southern latitudes. To further explore this relationship, the time series of monthly mean H_S, and the monthly H_S anomalies, averaged over the whole SH are plotted in Figure 5. The annual cycle is apparent with significant interannual variability observed. No correlation between the SH mean anomalies and climate indices tested (SOI, SAMI and IOD) is observed. If waves respond to pressure patterns regionally (as could be expected), then corresponding signals could easily be missed in the SH mean. To assess regional variations in the wave field, a principal components (EOF) analysis is carried out on the monthly mean altimeter-measured H_S fields.

Variability of altimeter derived wave heights is greatest during autumn and winter months, however we assess all seasons. An EOF analysis is carried out on seasonal datasets (DJF, MAM, JJA and SON). A total of 45 months for each seasonal dataset qualify in the

DOI: 10.1002/joc

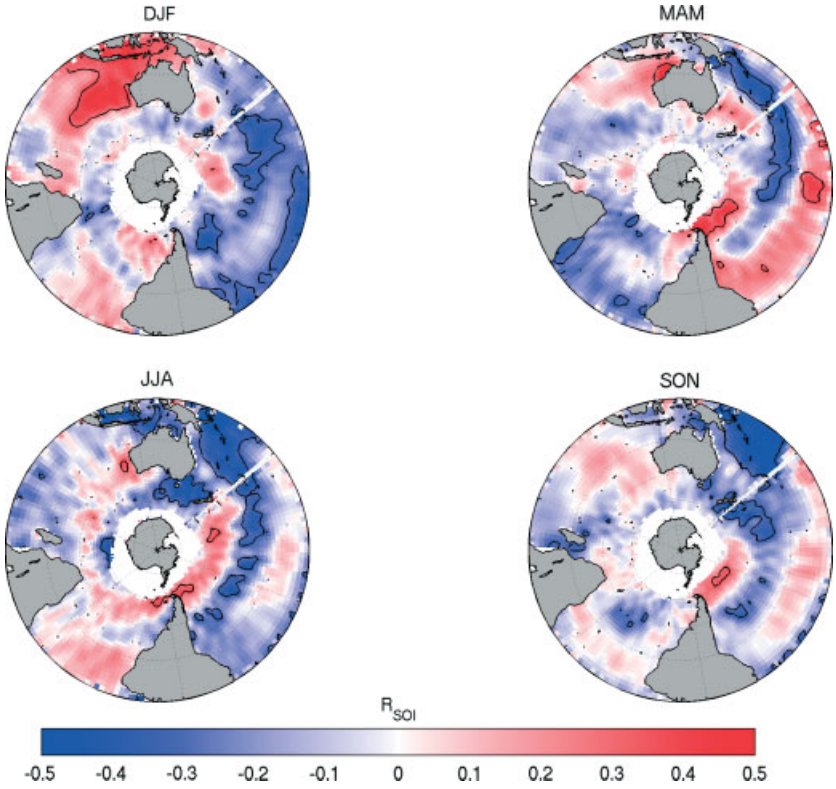

Figure 3. Correlation maps of seasonal mean H_S with Southern Oscillation Index for Summer (DJF); Autumn (MAM); Winter (JJA) and Spring (SON). Significant positive or negative correlations (at 95% confidence level) are bounded by solid black line.

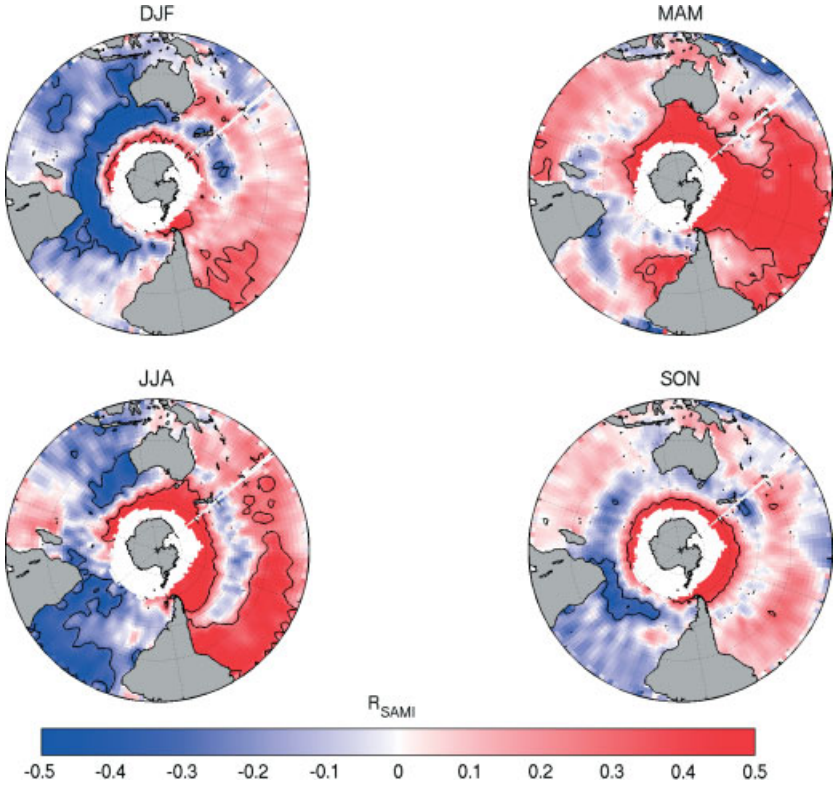

Figure 4. Correlation maps of seasonal mean H_S with Southern Annular Mode Index for Summer (DJF); Autumn (MAM); Winter (JJA) and Spring (SON). Significant positive or negative correlations (at 95% confidence level) are bounded by solid black line.

DOI: 10.1002/joc

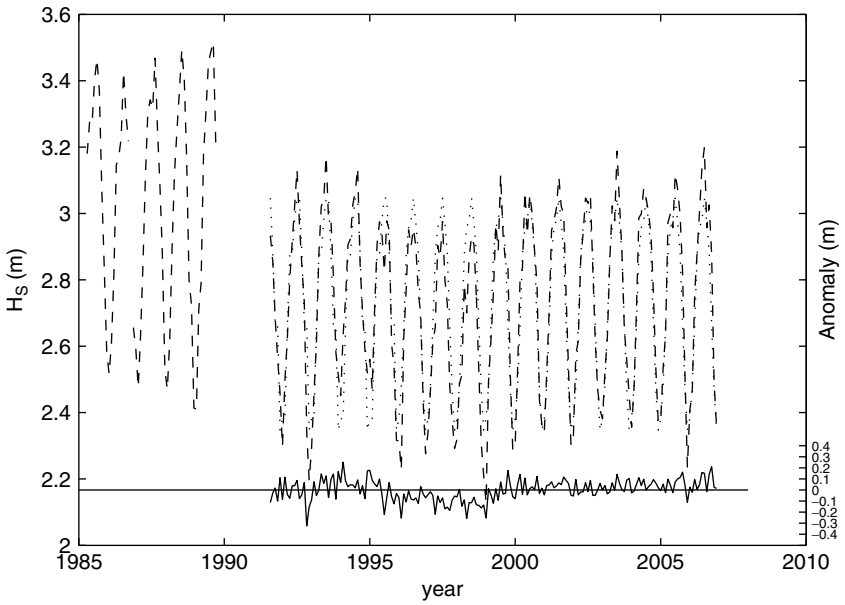

Figure 5. Time series of the monthly mean H_S (dash line), the mean annual cycle (dotted line), and the monthly anomalies (with the mean annual cycle removed from the signal; solid line); all averaged over the Southern Hemisphere.

post-1992 period. The time series (principle components) of the leading EOFs are determined for each seasonal dataset, and the variance explained by the EOFs, and the correlation of the principal components to climate indices SOI and SAMI are presented in Table IV. The first and second EOFs during MAM (describing 17 and 13% of the variance respectively) and winter (describing 19 and 12% respectively) show similar patterns (not shown), and similar significant correlations to the de-trended SAMI (Table IV). The first EOF for MAM and JJA displays larger wave heights in the Southern Ocean when the SAMI is larger ($R = 0.78$, MAM and $R = 0.58$, JJA; Figure 7a), particularly south of Australia and in the Pacific sector. The Atlantic and the region adjacent to south-west Australia show a decrease in wave heights with larger SAMI. The second EOF displays an increase in wave heights over all of the SH when the SAMI is larger, except for a small region in the south-east Pacific ($R = 0.16$, MAM and $R = 0.64$, JJA; Figure 7b). The observed trend in the Southern Ocean altimeter-measured H_S is consistent with the observed trend in the SAMI, whereby the Antarctic low pressure trough has shown a deepening, and consequently the Southern Ocean wind band has shifted further southwards and intensified. These observed trends have resulted in larger ocean waves in the Southern Ocean, which are then able to propagate throughout the world's oceans.

Table IV. Results of EOF analysis of altimeter-measured H_S.

Season	N	EOF	V	R (SAMI)	R (SOI)
DJF	16	1	17.2	−0.06	−0.13
		2	11.1	0.12	0.25
		3	8.1	−0.09	−0.21
		4	6.0	0.15	−0.17
MAM	15	1	17.5	**0.78**	−0.23
		2	13.0	0.16	−0.14
		3	11.7	0.11	−0.17
		4	6.1	−0.14	−0.23
JJA	15	1	19.0	**0.58**	**0.4**
		2	11.7	**0.64**	−0.21
		3	10.2	−0.28	−0.09
		4	6.5	−0.11	0.04
SON	14	1	16.9	−0.05	0.09
		2	14.5	0.06	0.13
		3	10.0	0.27	0.17
		4	8.6	−0.28	0.10

N is number of EOFs describing 80% of the variance. The first four EOFs for each seasonal anomaly set are shown. *V* is the percentage variance explained by each EOF. *R* (SAMI) is correlation between SAMI and principal component of the EOF. *R* (SOI) is the correlation between SOI and the principal component of the EOF. Bold text indicates significant correlation at 95% level.

4. Variability and trends of global wave model estimated wave energy flux

The shift in position of the storm belt and the location at which large waves are generated may have potential impacts on the direction of waves. The wave energy flux is a vector with magnitude being a function of the wave height squared and the wave period, and the direction is given by the direction the waves are travelling. We have used this statistic to describe the directional wave climate of the SH. Unfortunately, very little wave period and direction data are available in the SH, and consequently we rely on global wave models such as the ERA-40 re-analysis, and the corrected version produced by Sterl and Caires (2005). Another source is the operational global wave model NWW3 (Tolman *et al.*, 2002). Sterl and Caires (2005) identify a prominent dip in C-ERA-40 H_S

DOI: 10.1002/joc

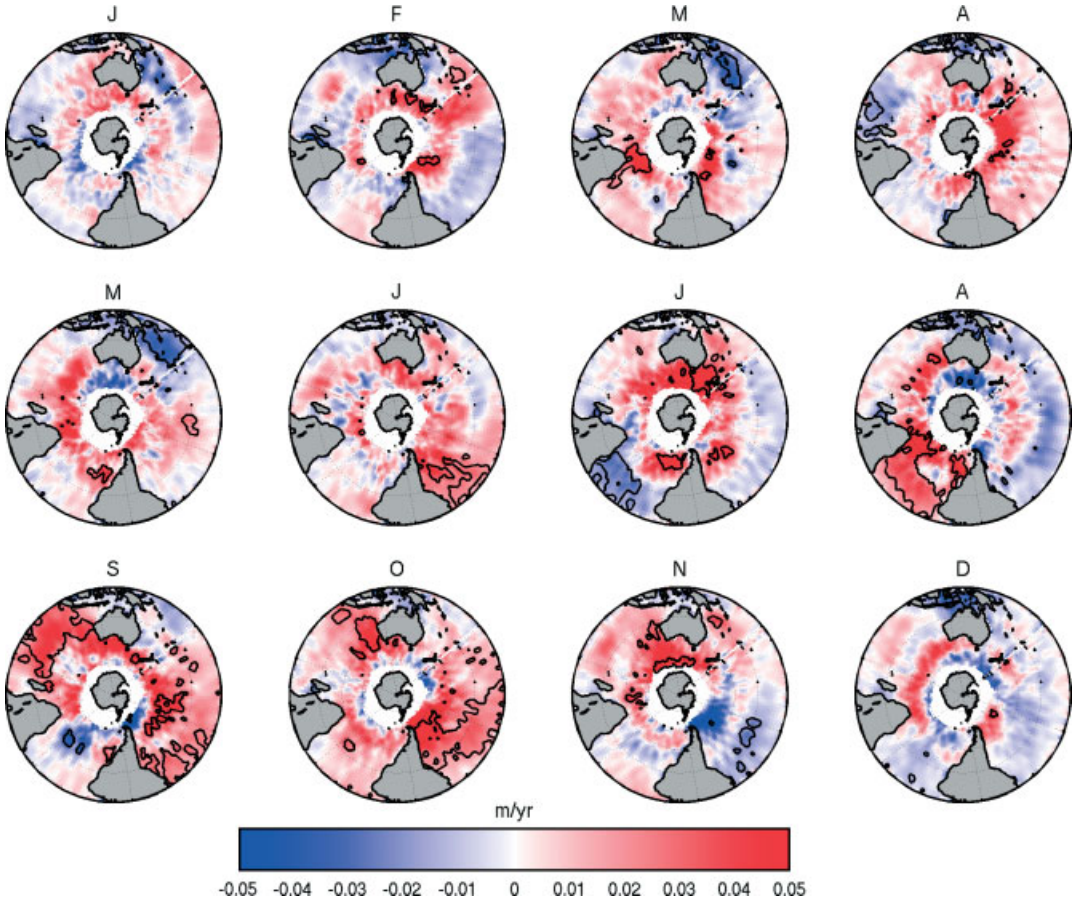

Figure 6. Trend in monthly mean altimeter derived H_S for period 1991–2006 for each month of the year (JFMAMJJASOND). Significant trends (at 95% confidence level) are bounded by a solid black line.

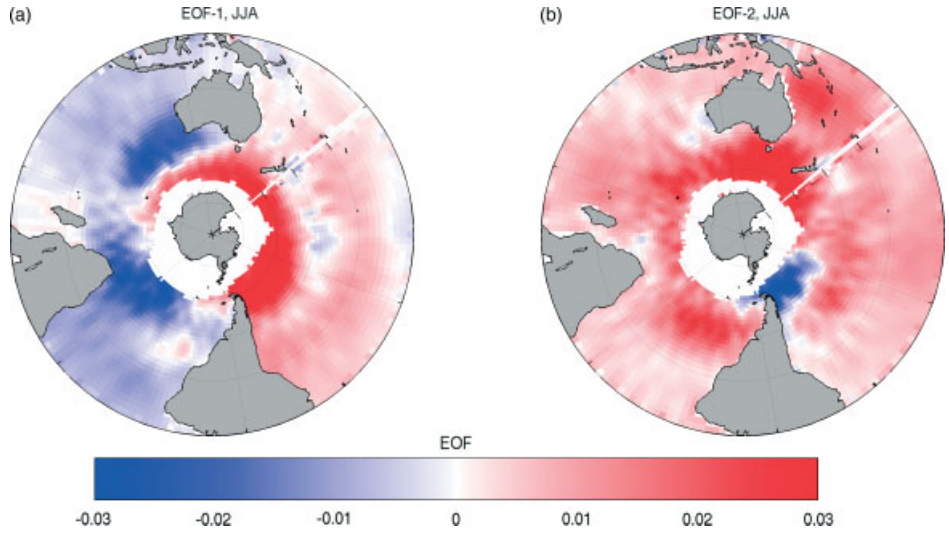

Figure 7. The first (a) and second (b) principal component of the winter (JJA) mean altimeter derived H_S.

in September 1975, which signals a change in regime with higher H_S observed after the dip than before. The dip in H_S is traced to a dip in wind speeds in the Pacific sector of the Southern Ocean and is suspected to be real. However, the change in the level before and after this dip was deemed to be most likely due to the assimilation of satellite data after 1979. As a result of this change in regime in this record, we have utilized only data from 1980 onwards (until end of 2001) in this study, making up a full 22 years of record.

Wave analyses typically use scalar statistical methods for wave heights and periods. In order to assist statistical calculations, the directional wave energy flux (E_F) is a vector, expressed here as a complex number $z = x + iy$.

DOI: 10.1002/joc

The real component of the wave energy flux vector, x, is the eastwards component, and the imaginary component, y, is the northwards component of the wave energy flux, such that the mean wave energy flux is given by:

$$\overline{z} = \frac{1}{n}\sum_{j=1}^{n} z_j = \overline{x} + i\overline{y} \tag{2}$$

And the variance of the wave energy flux is given by:

$$\sigma_z^2 = \sum_{j=1}^{n}(z_j - \overline{z})(z_j - \overline{z})^* = \sigma_x^2 + \sigma_y^2 \tag{3}$$

Where $z_j = x_j + iy_j$ is the complex representation of the wave energy flux vector for month j, $i^2 = -1$, (σ_x, σ_y, σ_z) are the standard deviation of (x, y, z) respectively, and the symbol (*) represents the complex conjugate. The wave energy flux has units of W/m wave crest.

Monthly mean wave energy flux magnitudes, directions and vector components were determined from the 22-year record of 6-hourly wave height, period and direction data. From these, the mean annual cycle, and seasonal and annual mean wave energy flux were determined for each of the 22 years. The seasonal directional variability found here is consistent with that from similar global wave models described by Young (1999). Seasonal and interannual variance of the wave energy flux at representative locations are presented in Table V. The greatest interannual variability (vector and magnitude variance) is observed at the Western Tasmania location. Directional variability is greatest in the SW Pacific Islands as a result of the seasonal monsoon/trade-wind reversal. Interannual variability in the length of the monsoon season leads to the high observed variability in the energy flux direction at this location.

The magnitude of the monthly mean wave energy flux (EF) was regressed against time. Large and significant positive trends (not shown) were observed throughout the SH. The spatial distribution of EF trends is similar to that for the altimeter measured H_S trends, but significant positive EF trends are observed in regions which display non-significant negative H_S trends in the altimeter-measured H_S record. To explore this further, we have determined 4-year mean H_S for the periods 1993–1996 and 1998–2001 from each of the altimeter-measured H_S, the C-ERA-40 H_S, and the original ERA-40 H_S data. The 1993–1996 4-year mean H_S is subtracted from the 1998–2001 4-year means H_S for each of the three cases to identify spatial patterns of positive and negative trends in each dataset. The spatial distribution of the trends is consistent between all datasets; i.e. regions displaying a positive trend in the altimeter-measured H_S data (Figure 8a) display very large positive trends in the ERA-40 dataset (Figure 8c); regions with no trend in Altimeter H_S data display a moderate positive trend in the ERA-40 data, and only regions with a very large negative trend in the Altimeter H_S data display a small negative trend in the ERA-40 data. We find that the trends in the ERA-40 H_S data over this period exceed the trend observed in the Altimeter H_S data. Although the trends in the C-ERA-40 data are nearer to the measured trends, the C-ERA-40 data also overestimate the positive trends in the SH H_S, and the area of negative trends is significantly reduced. To confirm that the reduced trend in the Altimeter data is not a feature of the sparse sampling of the altimeter, Figure 8b shows the trend in the C-ERA-40 H_S data having resampled the C-ERA-40 record as the Altimeters would have done. The trends in the sparsely sampled C-ERA-40 data (Figure 8b) are consistent with the non-sparsely sampled C-ERA-40 data (not shown). Each case displays significant increase in Southern Ocean wave heights, south of approximately 45 °S. The spatial extent of the impacts of these changes is recognized by wave height increases in regions where Southern Ocean swell has propagated. This signal can be seen in the eastern Pacific and Indian Oceans – locations where local wave generation is small but are subject to swell propagated from the Southern Ocean. Increase in the Southern Ocean generated swell can be expected to increase the mean wave period of the wave spectrum throughout the global ocean. Such increase in the mean wave period is observed in the ERA-40 dataset (Sterl and Caires, 2005),

Table V. Mean magnitude and direction of the wave energy flux, and measures of seasonal and interannual variance at selected sites.

Site	Lat	Long	$\lvert\overline{z}\rvert(\times 10^5)$ W/m	$\overline{\theta}$ °N	Seasonal			Interannual		
					σ_z $(\times 10^4)$ $(W/m)^2$	$\sigma_{\lvert z\rvert}$ $(\times 10^4)$ $(W/m)^2$	$\sigma_{\lvert e\rvert}$	σ_z $(\times 10^4)$ $(W/m)^2$	$\sigma_{\lvert z\rvert}$ $(\times 10^4)$ $(W/m)^2$	$\sigma_{\lvert e\rvert}$
West Tasmania	42.5 °S	142.5 °E	0.57	70.3	1.83	1.70	0.11	2.11	2.11	0.115
SW. Pac Islands	5 °S	185 °E	0.14	262.3	1.23	0.28	0.82	0.30	0.29	0.67
Cape Town	37.5 °S	17.5 °E	0.47	59.7	2.01	1.79	0.18	1.71	1.71	0.19
Chile coast	37.5 °S	282.5 °E	0.42	59.1	0.76	0.76	0.11	1.52	1.52	0.18
Tasman Sea	30 °S	155 °E	0.13	330.0	0.57	0.38	0.36	0.41	0.41	0.18
Maldives	2.5 °S	72.5 °E	0.16	352.9	0.83	0.82	0.09	0.56	0.56	0.50

σ_z is variance of wave energy flux vector, $\sigma_{|z|}$ is variance of magnitude of wave energy flux, and $\sigma_{|e|}$ is variance of the wave energy flux direction.

DOI: 10.1002/joc

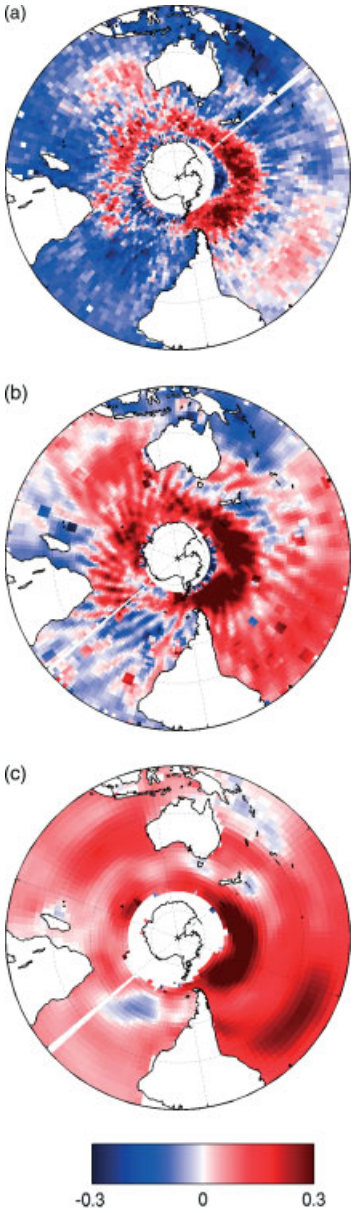

Figure 8. Difference in between 1998–2001 H_S mean, and the 1993–1996 H_S mean using (a) Altimeter derived H_S; (b) C-ERA-40 H_S; and (c) ERA-40 H_S. The C-ERA-40 data is resampled to be equivalent to Altimeter sampling. Colour scale is in metres difference between the two means.

but further attention is required to isolate the Southern Ocean generated swell component of this signal.

In contrast with significant wave height, we have no reason to suspect that the trends in wave direction are mis-represented in the ERA-40 dataset. At each of the directional waverider buoy sites, we compared the directional anomaly from the buoy data to the directional anomaly from the ERA-40 data. The difference between these anomaly time series has no significant trend, and therefore we conclude that the ERA-40 direction data do not exhibit any un-real trends. Figure 9 displays the directional distribution of the ERA-40 data, showing spatial histograms of the percentage of data for which waves are directed towards each of eight directional segments (N, NE, E, SE, S, SW, W, and NW). This directional distribution has been determined for each year of record, from 1980 to 2001, and the trend in the changing distributions determined (Figure 10). Key regions which exhibit shifts in wave direction are the Southern Ocean (where waves have shifted from north-westerly to westerly, or westerly to south-westerly), the Pacific Ocean, including the Tasman Sea, but mostly in the equatorial and eastern Pacific (where waves have shifted from south-easterly to southerly or southerly to south-westerly) and the equatorial Western Pacific (where waves have shifted from north-easterly to south-easterly), the Indian Ocean (where waves have shifted from westerly to south-westerly, south-westerly to southerly), and the southern Atlantic Ocean (where waves have shifted from south-westerly to southerly).

Directional shifts in the Tasman Sea wave climate have been shown to be statistically related to the SOI (Short *et al.*, 1995, 2000; Ranasinghe *et al.*, 2004; Goodwin, 2005). Wave direction is predominantly south-easterly during both phases of the El-Nino – Southern Oscillation, but these authors found that El-Nino (La Nina) events were related to a greater southerly (easterly) component to the waves, resulting in consequent clockwise (anti-clockwise) rotation of embayed beaches in Sydney's north (on the Australian east coast). For this study, the magnitude of the wave energy flux vector, and the eastward and northward directional components of the wave energy flux have been regressed against the SOI. Significant correlations between the eastward wave energy flux components and the SOI are observed throughout most of the Pacific Ocean, and during spring and summer months, significant correlation between the northward component of the wave energy flux and the SOI are observed (not shown). A negative anomaly of the SOI (i.e. an El-Nino event) is associated with an increase in the eastwards EF component (or weakening of the westward wave energy flux) in the tropical Pacific Ocean (Figure 11), associated with the weakening of the equatorial trade winds during El-Nino events. In the Tasman Sea both eastwards and northwards EF components have a negative correlation to the SOI. A negative SOI anomaly (El-Nino event) therefore results in the north-westward flux in this region gaining a greater northward component, and a decreased westward (increased eastwards) component – a clockwise rotation of the wave energy flux vector indicating waves shifting from south-easterly to southerly (consistent with Goodwin, 2005). This clockwise rotation is consistent with the rotation of beaches observed on the south-east Australian coastline during El-Nino events. Further north in the Coral Sea, the negative SOI anomalies are associated with a decrease in the eastwards component of the flux, observed as a strengthening of the south-easterly trade wind generated wave energy flux.

Over the past few decades, an increased number of El-Nino events have occurred relative to previous decades (Trenberth and Hoar, 1997; Mason, 2001). As El-Nino events are associated with a clockwise rotation of wave

DOI: 10.1002/joc

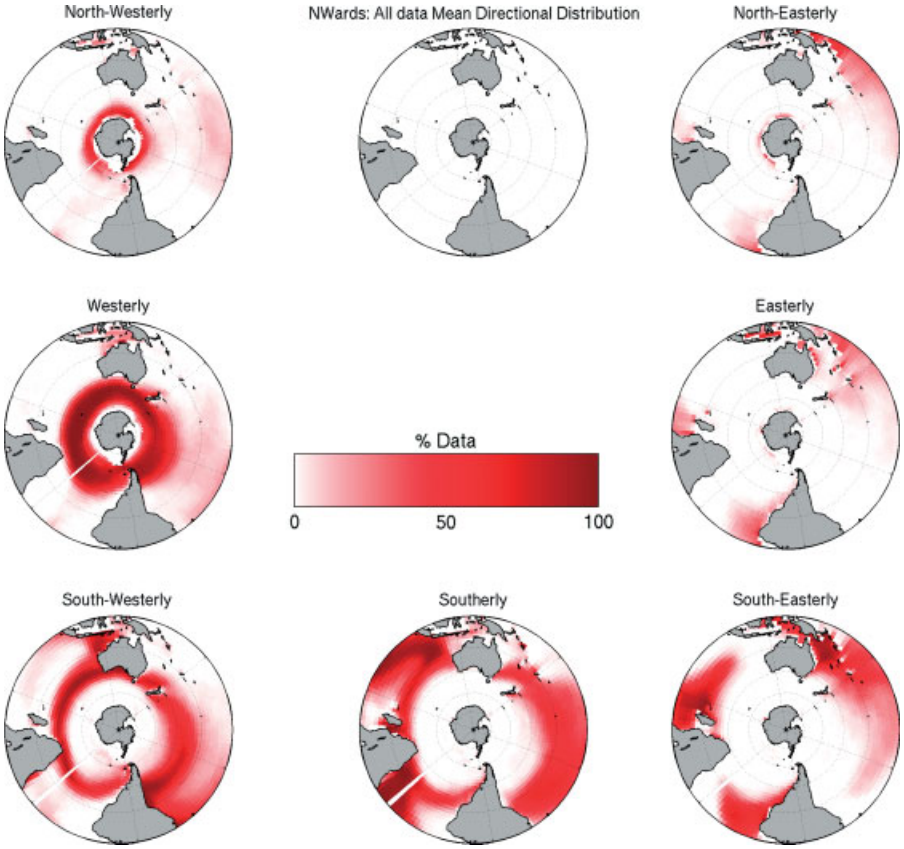

Figure 9. The directional distribution of Southern Hemisphere waves (ERA-40 derived wave direction). Each subplot displays a histogram indicating the percentage of wave data for waves are directed from that 45° directional segment. Colour scale is 0% of data in directional segment to 100% of data in directional segment.

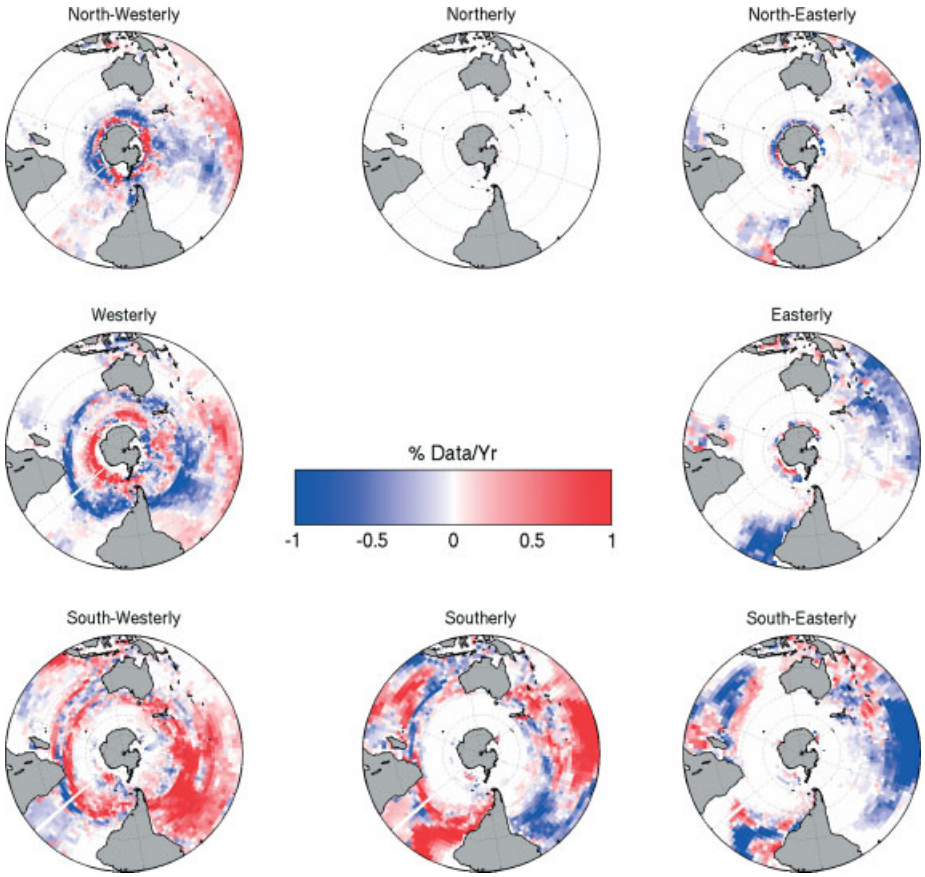

Figure 10. Trends in directional distribution of Southern Hemisphere waves (ERA-40 data, 1980–2001). Each subplot displays the gain/loss of wave data from each 45° directional segment over the 22-year record. Units are % of data/year of record.

DOI: 10.1002/joc

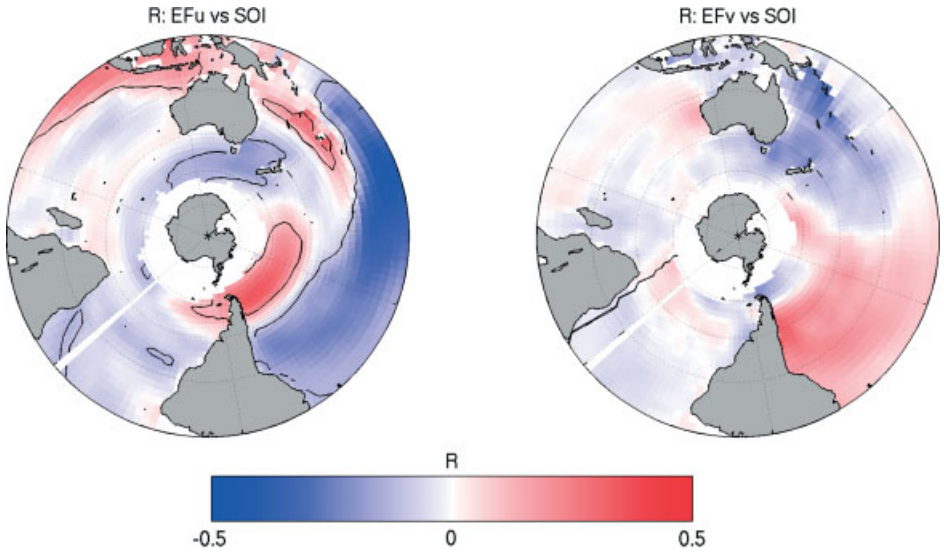

Figure 11. Correlation between the SOI and the eastwards and northwards components of the wave energy flux.

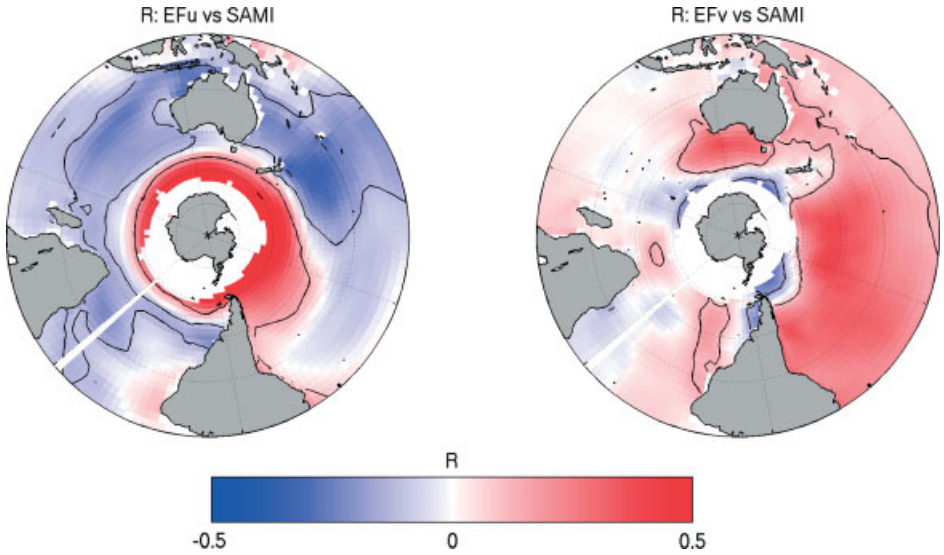

Figure 12. Correlation between the SAMI and the eastwards and northwards components of the wave energy flux.

direction in the south-western Pacific Ocean (Goodwin, 2005), the increase in El-Nino events is responsible for the clockwise rotation in wave direction observed in this region, over the period 1980–2001 (Figure 10).

In the far Southern Ocean (south of ∼48 °S), a significant positive correlation exists between the SAM and eastwards component of the wave energy flux (Figure 12), consistent with a strengthening and southwards shift of the Southern Ocean westerly winds. This shift is also reflected further north between latitudes 45–15 °S, where a significant negative correlation between the eastward flux component and SAM is observed over all longitudes bar the eastern Pacific and western Atlantic (which display a positive correlation). There is also a positive correlation between the northward flux component and the SAM in the region. These correlations together translate to an anti-clockwise rotation of the dominant north-eastward fluxes to have a greater northward component during positive phases of the SAM (waves are more southerly). The positive trend in the SAM over the past few decades (Marshall, 2003) therefore suggests an associated anti-clockwise directional shift in the wave energy flux along the southern and western margins of the Australian continent. The strength and direction of wave-driven currents along these coastlines are a characteristic of the direction of the incident deep-water waves, and their subsequent refraction over the continental shelf. An anti-clockwise rotation of the incident wave direction may lead to an expected increase in northward longshore transport which occurs along the western Australian margin (as observed by Masselink and Pattiaratchi, 2001), and an expected decrease in eastward longshore transport volumes along the southern Australian margin (as reported by Harvey, 1996; Hou *et al*.,

DOI: 10.1002/joc

2003). Variability in the sand budgets may lead to shift in the position of the shoreline in the form of erosion or accretion.

Significant positive correlations are observed between both of the wave energy flux directional components and the SAM in the eastern Pacific. This significant correlation in both components is consistent with the positive correlation observed between altimeters measured H_S and the SAM in the region, however an associated significant directional rotation is not resolved. We interpret this positive correlation between wave height in the eastern Pacific and the SAM to be a result of increased swell in the region, brought about via the intensifying storms in the Southern Ocean associated with positive anomalies of the SAM.

In Section 3, the regional variability of the altimeter-measured significant wave height was investigated using an EOF analysis. We have also carried out an EOF analysis on the wave energy flux vector field, using the method outlined by Preisendorfer (1988), to determine the dominant modes of directional variability and the regional variability of the wave energy flux anomalies (mean annual cycle removed) for each seasonal dataset. A total of 66 months for each seasonal dataset qualify in the 1980–2001 dataset. The time series (principle components) of the leading EOFs are determined for each seasonal dataset, and correlated to climate indices SOI and SAMI. These correlations and the variance explained by the EOFs are presented in Table VI.

Over all seasons, we observe a strong, and significant, correlation between the first EOF and the SAM (Table VI). These first EOFs all exhibit similar characteristics to those of MAM presented in Figure 13, which displays the strongest correlation to the SAM. Note that the two component (vector) EOF is a vector anomaly, and should be considered relative to the mean seasonal flux vectors. It can be seen (given the strong positive correlation to the SAM) that the variability in the SAM is associated with variance in wave energy flux in the Southern Ocean – most notably south of approximately 40 °S in the Indian and Pacific sectors. South of 50 °S and in the Indian sector of the Southern Ocean and south of Australia, a positive SAM anomaly is associated with a strengthening of the flux, with anti-clockwise rotation in direction. In the same latitude band in the Pacific sector, the same anomaly is also associated with a strengthening flux, but clockwise directional rotation. In the Indian Ocean, north of 50 °S, the positive SAM anomaly is associated with anti-clockwise directional rotation of the flux, and north of 45 °S, we observe that the SAM anomaly is also associated with a decrease in the magnitude of the flux. South of Australia (in the Great Australian Bight for example), we see that the wave energy flux increases in magnitude, and rotates anti-clockwise with a positive SAM anomaly. These general patterns of an anti-clockwise rotation, and increase in magnitude of the flux continue eastwards and northwards into the Tasman Sea and even the Coral Sea, along the eastern Australian Coast.

Table VI. Results of EOF analysis of wave energy flux vectors.

Season	N	EOF	V	R (SAMI)	R (SOI)
DJF	15	1	18.7	**−0.62**	**−0.31**
		2	14.4	−0.14	**−0.49**
		3	7.5	**0.63**	0.17
		4	6.4	**0.28**	−0.09
MAM	12	1	24.3	**0.87**	0.17
		2	12.0	−0.10	−0.16
		3	9.6	**0.32**	0.22
		4	6.6	**0.27**	−0.11
JJA	11	1	23.5	**−0.52**	−0.06
		2	13.9	−0.16	0.05
		3	11.4	**−0.26**	**0.50**
		4	7.7	0.07	0.02
SON	10	1	27.6	**−0.67**	**−0.31**
		2	16.2	**−0.59**	0.12
		3	10.2	**−0.44**	−0.05
		4	6.7	0.01	−0.10

N is number of EOFs describing 80% of the variance. EOF is EOF, showing first four EOFs for each seasonal anomaly set. *V* is variance explained by EOF. R (SAMI) is the correlation between SAMI and principal component R (SOI) with SOI. Bold text indicates significant correlation at 95% level

In the central South Pacific in the 35–50 °S latitude band, a positive anomaly of the SAM will result in anti-clockwise rotation of the energy flux, with little change in the magnitude; however, further east in the Pacific Ocean, the directional rotation will be small, but the magnitude of the flux could be expected to increase (Figure 13a). In addition to the first EOF displaying a correlation to the SAMI, we also observe that lower order EOFs (i.e. those which describe less of the variance) for all seasons also display significant correlations to the SAM (Table VI).

Correlation between the principle components of the EOFs of seasonal variability of the wave energy flux and the SOI are not as strong as to the SAMI. However, significant correlation with the SOI is observed for the leading EOF during SON and DJF. The variability forced by anomalies of the SOI could be expected to be greatest in the tropical Pacific (where the effects of El-Nino events are observed to be greatest). The EOF indicates that a negative anomaly of the SOI (an El-Nino event) is associated with a weakening and slight clockwise rotation, throughout the equatorial Pacific, consistent with the eastward shift in the convection cells of the Walker circulation which occurs during El-Nino events.

5. Discussion and conclusions

The effects of two principal modes of variability in the SH on the wave climate in the region have been investigated. The primary mode of both wave height and directional variability in the SH is correlated to the SAM. This variability is most apparent in the Southern Ocean, from which Southern Ocean generated swell propagate throughout all of the SH oceans.

DOI: 10.1002/joc

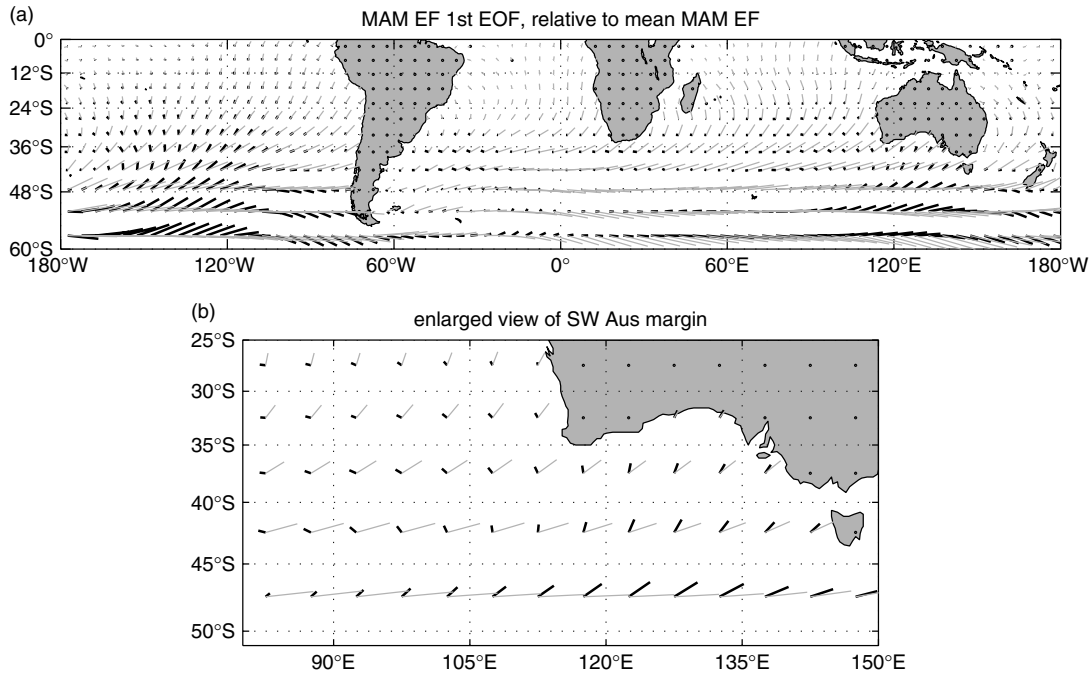

Figure 13. First EOF of autumn (MAM) wave energy flux vectors (grey vectors), using the 22-year ERA-40 dataset. Scaled autumn seasonal mean vectors (black vectors) are shown for directional reference. (a) Global view, and (b) is a zoomed in view of the south-west Australian margin, or Indian and Southern Ocean.

Trends in wave climate of the SH display strong regional variability. The wave climate in the South Pacific Ocean is shown to have strong correlation with both the SAM and the SOI. The variability associated with the trend in each of these indices (a positive trend in the SAMI over the past few decades and an increase in occurrence of El-Nino events) combine to produce trends in the South Pacific Ocean. H_S increases in the far Southern Ocean and decreases in the Western Pacific (in particular the Coral Sea). Wave direction rotates clockwise in the equatorial and mid-latitudes, and anti-clockwise in the far Southern Ocean.

The wave climate of the Tasman Sea, and the Western Pacific Ocean in general, displays a significant correlation to the SO Index, and the occurrence of El-Nino/La Nina events, with a clockwise rotation of wave direction during negative anomalies of the SOI (El-Nino events). These results confirm previously published results (e.g. Ranasinghe *et al*., 2004; Goodwin, 2005) using different but complementary methods.

In the Indian Ocean Sector of the Southern Ocean, wave climate variability is correlated with the SAM, particularly during autumn and winter months. Positive trends in H_S and anti-clockwise directional trends in the far Southern Ocean (south of $\sim$48 °S) are attributed to the positive trend in the SAM. The wave climate in the South Atlantic Ocean displays very little variability, escaping the influence of the SAM. The shadowing influence of the South American continent may be the dominant factor here, blocking storm systems which propagate around the southern latitudes, and reducing the propagation of swell from other Southern Ocean extra-tropical storms.

The relationship between the SAM and the Southern Ocean wave climate has not been previously described. Sterl and Caires (2005) described significant trends in the significant wave heights of the Southern Ocean (from the ERA-40 waves re-analysis), and indicated that the driver of the significant trends was an increased number of storms in the Southern Ocean. A southern intensification of the Southern Ocean storm belt associated with the SAM has been previously described, and it has been speculated (Hemer *et al*., 2008) that such a shift in location and intensification of the Southern Ocean storms would have an impact on the properties of the waves observed in buoy records along the southern Australian margin. In this study, it is seen that the positive trend in the SAM observed over the past few decades has been associated with an increase in wave heights in the far Southern Ocean and the mid-latitudes of the eastern Pacific Ocean during the autumn and winter months. From EOF analysis, the principle mode of variability in the SH directional wave climate is shown to have a strong significant correlation to the SAM. Possibly the most marked feature of this relationship is the anti-clockwise rotation of the wave direction in the region south and west of the Australian continent. Increases in Southern Ocean generated waves, partly attributed to the SAM, may be observed to propagate throughout the world's oceans. The effects of such changes on surface wave period, expected to increase with the greater swell component, needs further attention to identify the spatial extent of the impacts of these changes, particularly on the coastal zone.

Understanding the relationship between the SH wave climate and the SAM enables estimates of changes

DOI: 10.1002/joc

under future climate scenarios. General circulation model (GCM) simulations forced with Antarctic ozone depletion display a positive increase in the SAM (Gillett and Thompson, 2003). Similarly, models forced by increasing (well-mixed) greenhouse gases also respond with an increase in the SAM (Cai *et al*., 2003). These scenarios can consequently be expected to result in continuing observed trends in the Southern Ocean wave climate including wave height increases and directional rotation. Scenarios including a stabilization of greenhouse gas emissions result in a reversal of the existing trend in the SAM (Cai *et al*., 2003). Similarly, Shindell and Schmidt (2004) force a GCM with combined greenhouse gas increases, and stratospheric ozone recovery, where the influence of these two factors on the SAM oppose one another. Their findings show continuing SAM-like zonal structure in the mid-troposphere and above due to the greenhouse gas forcing, the surface circulation, which controls the wave climate, displays minimal trend.

Wave-driven currents are the primary mechanism for sand transport in the coastal zone. The strength and direction of these currents are dependent on the direction of the waves off the continental shelf. For example, the most widely used equation for longshore sediment fluxes, Q_S, is known as the CERC equation (Komar and Inman, 1970; Komar, 1998):

$$Q_S = K_1 {H_b}^{5/2} \sin(\phi_b - \theta)\cos(\phi_b - \theta) \qquad (4)$$

Where H_b and ϕ_b are breaking wave height and crest angle, respectively, θ is the local shoreline orientation, and K_1 is an empirical constant. Therefore, given constant wave height, longshore sediment fluxes will increase as wave direction tends away from orthogonality. A 20° shift in direction will therefore result in large changes in the longshore transport flux (for example, if wave direction is 10° off orthogonal, a 20° shift in direction can result in a reversal of longshore flux along the coast (10° other side of orthogonal), or alternatively increase the longshore transport volume by a factor of 2.5 (to 30° from orthogonal). Shifts of such magnitude in the longshore sediment flux will produce notable change in the coastal sediment budget. Shifts in the position of the shoreline (via coastal erosion or accretion) are attributed to such changes in the coastal sediment budget, and consequently, it is important to quantify the directional variance attributed to different modes of variability in the world's oceans.

To illustrate the effects of the directional variance of waves along the south-western Australian margin associated with the SAM, the autumn directional wave climate is reconstructed using the first, third and fourth EOFs of the MAM directional wave climate anomalies (which each display a significant correlation to the SAM). The directional variance quantified in this reconstruction is equivalent to approximately 20° change in wave direction in the region to the west of the Australian continent. Using a ray-tracing model to track waves across the continental shelf in this region, we find 20° change in offshore wave direction remains of the order 20° change in wave direction at the coast. Given mean wave direction is near to orthogonal to the coast in this region (similar to the example given above), variability in wave direction of this magnitude can result in a north–south switch of the longshore wave-driven current along the coast, or significant changes in the magnitude of the longshore sediment fluxes.

Measurements of longshore sediment fluxes are even more scarce than *in situ* wave data in the SH, and therefore the ability to track interannual variability and trends in such data is impossible. Interpretation of such variability is restricted to shoreline monitoring programmes (e.g. beach profile measurements such as those carried out by Short *et al*. (1995, 2000)), which are few and far between. It is hoped that this study can stimulate interest in similar programmes to determine the measured effect of wave direction, and its relationship to the SAM, on shoreline position along the southern and western Australian margin, and elsewhere in the SH. Such monitoring programmes will benefit further modelling of climate change and consequent shoreline response to enable better adaptation to future coastal changes.

Acknowledgements

This paper is contribution to the Commonwealth Scientific Industrial Research Organisation (CSIRO) Climate Change Research Program and Wealth from Oceans Flagship. The research was funded with assistance from the Australian Government Department of Climate Change and supported by the Australian Government's Cooperative Research Centres Programme through the Antarctic Climate and Ecosystems Cooperative Research Centre. The authors acknowledge the supply of data from: ECMWF; Andreas Sterl, KNMI; DEOS, TU Delft; Australian Governement Bureau of Meteorology; Manly Hydraulics Laboratory, Department of Commerce, Government of New South Wales; Department of Planning and Infrastructure, Government of Western Australia; Environmental Protection Agency, Government of Queensland; Port of Melbourne; and Environment Canterbury, New Zealand. We also thank Dr Jim Gunson (CSIRO Marine and Atmospheric Research), Dr Peter Adams (University of Florida) and one anonymous reviewer for their comments that contributed to the manuscript. The Centre for Australian Weather and Climate Research is a partnership between CSIRO and the Australian Bureau of Meteorology.

References

Bacon S, Carter DJT. 1991. Wave climate changes in the North Atlantic. *International Journal of Climatology* **11**: 545–558.

Cai WJ, Whetton PH, Karoly DJ. 2003. The response of the Antarctic Oscillation to increasing and stabilised CO2. *Journal of Climate* **16**: 1525–1538.

DOI: 10.1002/joc

Caires S, Sterl A. 2005. A new non-parametric method to correct model data: application to significant wave height from the ERA-40 reanalysis. *Journal of Atmospheric and Oceanic Technology* **22**(4): 443–459.

Challenor PG, Cotton PD. 2002. The joint calibration of altimeter and in-situ wave heights. Technical Report No. 13, World Meteorological Organization document number WMO/TD-No.1081, JCOMM.

Cotton PD. 1998. *A feasibility study for a global satellite buoy intercalibration experiment*. Southampton Oceanography Centre Resolution Consultation Report No. 26, Southampton Oceanography Centre, Southampton, UK, 73.

Cotton PD, Carter DJT. 1994. Cross calibration of TOPEX, ERS-1, and Geosat wave heights. *Journal of Geophysical Research* **99**: 25025–25033, [Correction:1995. *Journal of Geophysical Research* **100**: 7095].

Cox AT, Swail VR. 2001. A Global Wave Hindcast over the Period 1958-1997: Validation and Climate Assessment. *JGR (Oceans)*, **106**(C2): pp. 2313–2329.

Gillett NP, Thompson DWJ. 2003. Simulation of recent Southern Hemisphere climate change. *Science* **302**: 273–275.

Gillett NP, Kell TD, Jones PD. 2006. Regional climate impacts of the Southern Annular Mode. *Geophysical Research Letters* **33**: L23704. DOI:10.1029/2006GL027721.

Gong D, Wang S. 1999. Definition of Antarctic oscillation index. *Geophysical Research Letters* **26**: 459–462.

Goodwin I. 2005. A mid-shelf, mean wave direction climatology for south-eastern Australia, and it's relationship to the El-Nino – Southern Oscillation since 1878 A.D. *International Journal of Climatology* **25**: 1715–1729.

Gorman RM, Bryan KR, Laing AK. 2003. Wave hindcast for the New Zealand region: deep-water wave climate. *New Zealand Journal and Marine and Freshwater Research* **37**: 589–612.

Graham NE. 2003. Variability in the wave climate of the North Pacific: links to inter-annual and inter-decadal variability. In: *Oceans 2003 Conference*. San Diego: Marine Technology Society, pp. 969–972.

Harvey N. 1996. The significance of coastal processes for management of the River Murray Estuary. *Australian Geographical Studies* **34**(1): 45–57.

Hemer MA, Church JA, Hunter JR. 2007. Waves and climate change on the Australian Coast. *Journal of Coastal Research* **50**: 432–437.

Hemer MA, Simmonds I, Keay K. 2008. A classification of wave generation characteristics during large wave events on the Southern Australian margin. *Continental Shelf Research* **28**: 634–652.

Holthuijsen LH. 2007. *Waves in Oceanic and Coastal Waters*. Cambridge University Press: Cambridge, 387.

Hou B, Frakes LA, Alley NF, Heithersay P. 2003. Evolution of beach placer shorelines and heavy mineral deposition in the eastern Eucla Basin, South Australia. *Australian Journal of Earth Sciences* **50**(6): 955–965.

Hurrell JW, van Loon H. 1994. A modulation of the atmospheric annual cycle in the Southern Hemisphere. *Tellus* **46A**: 325–338.

Kidson JW. 1999. Principal modes of Southern Hemisphere low-frequency variability obtained from NCEP-NCAR re-analyses. *Journal of Climate* **12**: 2808–2830.

Komar PD. 1998. *Beach Processes and Sedimentation*. Simon and Schuster: Upper Saddle River.

Komar PD, Inman DL. 1970. Longshore sand transport on beaches. *Journal of Geophysical Research* **75**: 5914–5927.

Laing AK. 2000. New Zealand wave climate from Satellite observations. *New Zealand Journal of Marine and Freshwater Research* **34**: 727–744.

Marshall GJ. 2003. Trends in the southern annular mode from observations and reanalyses. *Journal of Climate* **16**: 4134–4143.

Mason SJ. 2001. El Nino, climate change and the Southern African climate. *Environmetrics* **12**: 327–345.

Masselink G, Pattiaratchi CB. 2001. Seasonal changes in beach morphology along the sheltered coastline of Perth, western Australia. *Marine Geology* **172**: 243–263.

Naeije MC, Schrama EJO, Scharroo R. 2000. The radar Altimeter Database System project RADS. In: Tammy I. Stein (eds); Proceedings of the IGARSS 2000 conference (Hawaii, 2000-07-24), pp. 487–490, ISBN: 7803-6357-0.

Petkovic P, Buchanan C. 2002. *Australian Bathymetry and Topography Grid (digital dataset)*. Geoscience Australia: Canberra.

Power S, Casey T, Folland C, Colman A, Mehta V. 1999. Inter-decadal modulation of the impact of ENSO on Australia. *Climate Dynamics* **15**: 319–324.

Preisendorfer RW. 1988. *Principal Components Analysis in Meteorology and Oceanography*. Elsevier: The Netherlands.

Queffeulou P. 2004. Long-term validation of wave height measurements from altimeters. *Marine Geodesy* **27**: 495–510.

Ranasinghe R, McLoughlin R, Short A, Symonds G. 2004. The Southern oscillation index, wave climate and beach rotation. *Marine Geology* **204**: 273–287. DOI:10.1016/S0025-3227(04)00002–7.

Saji NH, Goswami BN, Vinayachandran PN, Yamagata T. 1999. A dipole mode in the tropical Indian Ocean. *Nature* **401**: 360–363.

Sasaki W, Iwasaki SI, Matsuura T, Iizuka S, Watabe I. 2005. Changes in wave climate off Hiratuska, Japan, as affected by storm activity over the western North Pacific. *Journal of Geophysical Research* **110**: C09008. DOI:10.1029/2004JC002730.

Scott D, Resio D, Pantoja C. 2002. Swell propagation and nearshore wave climate. *7th International Workshop on Wave Hindcasting and Forecasting*, Meteorological Service of Canada, 13–24.

Shindell DT, Schmidt GA. 2004. Southern Hemisphere climate response to ozone changes and greenhouse gas increases. *Geophysical Research Letters* **31**: L18209. DOI: 10.1029/2004GL020724.

Short AD, Trenaman NL. 1992. Wave climate of the Sydney region; an energetic and highly variable ocean wave regime. *Australian Journal of Marine and Freshwater Research* **43**: 765–791.

Short AD, Cowell PD, Cadee M, Hall W, van Dijke B. 1995. Beach rotation and possible relation to the Southern oscillation. *Proceedings of the Ocean and Atmosphere Pacific International Conference*. National Tidal Facility, Adelaide, 329–334.

Short AD, Trembanis AC, Turner I. 2000. Beach oscillation, rotation and the Southern oscillation, Narrabeen Beach, Australia. *Proceedings of the 27thInternational Coastal Engineering Conference*. ASCE: Sydney; 2439–2452.

Simmonds I, Keay K. 2000. Variability of Southern Hemisphere extra-tropical cyclone behaviour, 1958-97. *Journal of Climate* **13**: 550–561.

Snodgrass FE, Groves GW, Hasselmann K, Miller GR, Munk WH, Powers WH. 1966. Propagation of ocean swell across the Pacific. *Philosophical Transactions of the Royal Society of London* **249A**: 431–497.

Sterl A, Caires S. 2005. Climatology, variability and extrema of ocean waves: the web-based KNMI/ERA-40 wave atlas. *International Journal of Climatology* **25**(7): 963–977.

Swail VR, Cox AT. 2000. On the use of NCEP-NCAR reanalysis surface marine wind fields for a long term North Atlantic wave hindcast. *Journal of Atmospheric and Oceanic Technology* **17**: 532–545.

Swail VR, Komen G, Ryabinin V, Holt M, Taylor PK, Bidlot J. 2001. Waves in the global ocean observing system. *Observing the Oceans in the 21st Century*, Koblinsky CJ, Smith NR (eds) Uniprint: Melbourne, Australia;, 149–176.

Thompson DWJ, Solomon S. 2002. Interpretation of recent Southern Hemisphere climate change. *Science* **296**: 895–899.

Tolman HL, Balasubramaniyan B, Burroughs LD, Chalikov DV, Chao YY, Chen HS, Gerald VM. 2002. Development and implementation of wind generated ocean surface wave models at NCEP. *Weather and Forecasting* **17**: 311–333.

Trenberth KE, Hoar TJ. 1997. El Nino and climate change. *Geophysical Research Letters* **24**(23): 3057–3060.

Wang XL, Swail VR. 2001. Changes of extreme wave heights in northern hemisphere oceans and related atmospheric circulation regimes. *Journal of Climate* **14**: 2204–2221.

Wolf J, Woolf DK. 2006. Waves and climate change in the north-east Atlantic. *Geophysical Research Letters* **33**: L06604. DOI:10.1029/2005GL025113.

Woolf DK, Challenor PG, Cotton PD. 2002. Variability and predictability of the North Atlantic wave climate. *Journal of Geophysical Research* **107**(C10): 3145. DOI:10,1029/2001JC001124.

Young IR. 1999. Seasonal variability of the global ocean wind and wave climate. *International Journal of Climatology* **19**: 931–950.